

1 **BrGDGTs-based seasonal paleotemperature reconstruction for the last 15,000 years**
2 **from a shallow lake on the eastern Tibetan Plateau**

3 Xiaohuan Hou ^a, Nannan Wang ^a, Zhe Sun ^b, Kan Yuan ^{a, c}, Xianyong Cao ^a, Juzhi Hou ^{a*}

4 ^a *Group of Alpine Paleocology and Human Adaptation (ALPHA), State Key Laboratory of Tibetan*
5 *Plateau Earth System, Resources and Environment (TPESRE), Institute of Tibetan Plateau Research,*
6 *Chinese Academy of Sciences, Beijing 100101, China*

7 ^b *Institute of Geography and Resources Science, Sichuan Normal University, Chengdu, 610066, China*

8 ^c *University of Chinese Academy of Sciences, Beijing 100049, China*

9

10 * Corresponding author

11 E-mail address: houjz@itpcas.ac.cn

12

13 **ABSTRACT**

14 Knowledge of Holocene temperature changes is crucial for addressing the problem of the
15 discrepancy between Holocene proxy temperature reconstructions and climate model
16 simulations. The complex spatiotemporal pattern of temperature variations on the Tibetan
17 Plateau (TP) further complicates the study of Holocene continental climate change. The
18 discrepancy between model-based and proxy-based Holocene temperature reconstructions
19 possibly results from the seasonal biases and environmental ambiguities of the proxies.
20 Quantitative temperature reconstructions using different proxies from the same sediment core
21 can provide an effective means of evaluating different proxies; however, this approach is
22 unusual in terrestrial environments. Here, we present an ice-free-season temperature record
23 for the past 15 ka from a shallow, freshwater lake on the eastern TP, based on brGDGTs
24 (branched glycerol dialkyl glycerol tetraethers). This record shows that the Holocene Thermal
25 Maximum lags the pollen-based July temperature recorded in the same sediment core. We
26 conclude that the mismatch between the brGDGTs-based and pollen-based temperatures is
27 primarily the result of seasonal variations in solar irradiance. The overall pattern of
28 temperature changes is supported by other summer temperature records, and the Younger
29 Dryas cold event and the Bølling–Allerød warm period are also detected. A generally warm
30 period occurred during 8–3.5 ka, followed cooling in the late Holocene. Our findings have
31 implications for understanding the seasonal signal of brGDGTs in shallow lakes, and provide
32 critical data for confirming the occurrence of seasonal biases in different proxies from high-
33 elevation lakes. To further investigate the significance of the brGDGTs and temperature
34 patterns on the TP, we reviewed previously published brGDGTs-based Holocene temperature

35 records across the TP. The results demonstrate that brGDGTs have been employed to
36 reconstruct various temperatures in different studies, including annual average temperature
37 and warm-biased temperature, and that both show a gradual warming trend during the
38 Holocene with relatively cooler conditions during the middle Holocene, and a cooling trend
39 during the middle to late Holocene. We analyzed the possible reasons for the diverse
40 brGDGTs records on the TP and emphasize the importance of considering lake conditions
41 and modern investigations of brGDGTs in lacustrine systems when using brGDGTs to
42 reconstruct paleoenvironmental conditions.

43 **Keywords:** Tibetan Plateau, brGDGTs, the mean temperature of Months Above Freezing,
44 shallow lake, Holocene

45 **1 Introduction**

46 Global climate change has had a profound impact on both the natural ecological and socio-
47 economic systems that are vital for human survival and development, making climate change
48 a critical limiting factor for the sustainable development of human society. The Tibetan
49 Plateau (TP), also called the “Third Pole” (Qiu, 2008), has undergone a more rapid warming
50 over the last five decades, with a rate twice that of the global average (0.3 – 0.4°C/decade)
51 (Chen et al., 2015; Kuang and Jiao, 2016), making it one of the world's most temperature-
52 sensitive regions (Chen et al., 2015; Yao et al., 2022). Consequently, assessing the impact of
53 future climate change on the TP is becoming increasingly important. To enhance the
54 precision and accuracy of future climate change estimates for the TP under ongoing global
55 climate change and to minimize the uncertainty in climate simulations, it is essential to
56 investigate the processes and mechanisms of regional climate and environmental changes,

57 with particular emphasis on temperature, on a relatively long timescale, such as that of the
58 Holocene.

59

60 The Holocene, the most recent geological epoch, is closely linked with the development of
61 human civilization. Quantitative reconstructions of Holocene temperature trends can be used
62 to explore their impacts on civilization and to establish a geological and historical context for
63 predicting future climate changes. In recent decades, many Holocene quantitative
64 reconstructions of seasonal and annual temperatures for the TP have been produced using
65 various proxies, like pollen (Herzschuh et al., 2014; Lu et al., 2011), chironomids (Zhang et
66 al., 2017; Zhang et al., 2019a), $\delta^{18}\text{O}$ in ice cores (Pang et al., 2020; Thompson et al., 1997),
67 and biomarkers (Cheung et al., 2017; Hou et al., 2016; Zhao et al., 2013). These
68 reconstructions have provided crucial data for the elucidation of Holocene temperature
69 changes. However, the available Holocene temperature records from the TP show divergent
70 trends. Multiple proxy indicators indicate three different Holocene temperature patterns on
71 the TP. First, a consistent Holocene warming trend (Feng et al., 2022; Opitz et al., 2015; Sun
72 et al., 2022). For example, brGDGTs based annual temperatures (Feng et al., 2022; Sun et al.,
73 2022) indicate a gradual warming trend which resembles the $\delta^{18}\text{O}$ temperature record from
74 the Chongce ice core on the western TP, except for the last 2 ka (Pang et al., 2020). Second,
75 an early to middle Holocene summer temperature maximum and a gradual cooling trend
76 during the late Holocene are observed in pollen-, alkenone- and chironomid-based
77 temperature records (Herzschuh et al., 2014; Hou et al., 2016; Wang et al., 2021a; Zhang et
78 al., 2017; Zheng et al., 2015). Third, a prominent relatively cool middle Holocene (Li et al.,
79 2017; Wang et al., 2021c); for example, a composite temperature record suggests that

80 temperatures were $\sim 2^{\circ}\text{C}$ cooler during the middle Holocene than during the early and late
81 Holocene (Wang et al., 2021c). Several records also show a steady long-term trend without
82 distinct cooling or warming (Sun et al., 2021). Moreover, the cooling trends in proxy-based
83 Holocene temperature records are inconsistent with those of climate models, which indicate a
84 warming trend, and this inconsistency is widely known as the “Holocene temperature
85 conundrum” (Liu et al., 2014). There are several potential factors that may contribute to the
86 disparity in Holocene temperature trends, including seasonal biases and uncertainties in
87 temperature proxies and reconstructions, independent of climate models (Bova et al., 2021;
88 Cartapanis et al., 2022; Hou et al., 2019; Liu et al., 2014; Marsicek et al., 2018). While
89 several recent studies have suggested that seasonality in proxies is not the major cause of the
90 Holocene temperature conundrum (Dong et al., 2022; Zhang et al., 2022b), it is significant
91 that the TP is an alpine and high-altitude region with significant seasonal temperature
92 variations. Moreover, most organisms tend to grow during the warmer seasons at high
93 latitudes and high altitudes (Zhao et al., 2021a). Currently, however, we lack unambiguous
94 and reliable seasonal temperature records to support a seasonality-bias hypothesis. Extensive
95 research has been conducted in lakes, employing a single proxy to reconstruct past
96 temperature fluctuations. However, there have been scarce studies that employ various
97 proxies within the same core to reconstruct paleotemperature variations. Furthermore, the
98 limited number of studies primarily concentrate on reconstructing summer temperature and
99 annual average temperature. For example, a chironomid-based July temperature
100 reconstruction for Tiancai lake on the southeastern TP shows higher temperatures during the
101 early to middle Holocene (Zhang et al., 2017), while the brGDGTs-based annual average

102 temperature shows a warming trend (Feng et al., 2022). Different proxies may reflect the
103 seasonal temperatures in different months, and thus producing temperature reconstructions
104 for different months for the same sediment core may help better understand the seasonal bias
105 of terrestrial temperature records. Furthermore, the reconciliation of the divergent trends of
106 Holocene temperature on the TP and its surroundings requires additional high-altitude
107 temperature records from these regions, with reliable chronologies and proxy records with an
108 unambiguous climatological significance.

109
110 Branched glycerol dialkyl glycerol tetraethers (brGDGTs) are a group of membrane-spanning
111 lipids found in bacteria (Fig. S1) (Chen et al., 2022; Halamka et al., 2022; Sinninghe Damsté
112 et al., 2000), and they have become a powerful tool for quantifying past terrestrial
113 temperature variations. Through investigations of brGDGTs in globally-distributed soils, it
114 was found that the distribution of brGDGTs is primarily related to temperature and pH
115 (Weijers et al., 2007). Subsequently, brGDGTs–temperature calibrations from soil, peat and
116 lake sediments were established on scales from global (Crampton-Flood et al., 2020; De
117 Jonge et al., 2014; Martínez-Sosa et al., 2021; Weijers et al., 2007) to regional (e.g., East Asia)
118 (Dang et al., 2018; Ding et al., 2015; Sun et al., 2011; Wang et al., 2016), leading to
119 considerable progress in reconstructing terrestrial temperatures, particularly on the TP
120 (Cheung et al., 2017; Li et al., 2017; Zhang et al., 2022a).

121
122 Natural lakes are widely distributed across the TP (Zhang et al., 2019b). Lake sediments,
123 characterized by their organic matter-rich composition, exhibit continuous and rapid

124 accumulation rates. As a result, they offer high-resolution records of environmental changes,
125 making them highly valued as a primary terrestrial climate archive (Moser et al., 2019).
126 BrGDGTs in lacustrine systems are often more strongly correlated with temperature, with
127 higher coefficient of determination (r^2) and lower root mean square error (RMSE) values
128 (Martínez-Sosa et al., 2021), than in soils and peats. However, the factors that impact the
129 distribution of brGDGTs in lakes are intricate and multidimensional. Notably, the sources of
130 brGDGTs within lakes are intricate, involving contributions from soil as well as
131 autochthonous lake processes. Moreover, an expanding body of research underscores a
132 substantial prevalence of autochthonous brGDGTs in lakes (Tierney and Russell, 2009;
133 Tierney et al., 2010; Wang et al., 2021b; Weber et al., 2015). Furthermore, the origins of
134 brGDGT producers remain uncertain and could be influenced by various factors, including
135 lake salinity (Wang et al., 2021b), redox conditions (Weber et al., 2018), oxygen content
136 and/or mixing patterns (Buckles et al., 2014; van Bree et al., 2020; Wu et al., 2021).
137 Additionally, even lake depth plays a role due to distinct ecological niches (Woltering et al.,
138 2012), thereby contributing to the intricate interplay that shapes the distribution of brGDGTs
139 within lakes.

140

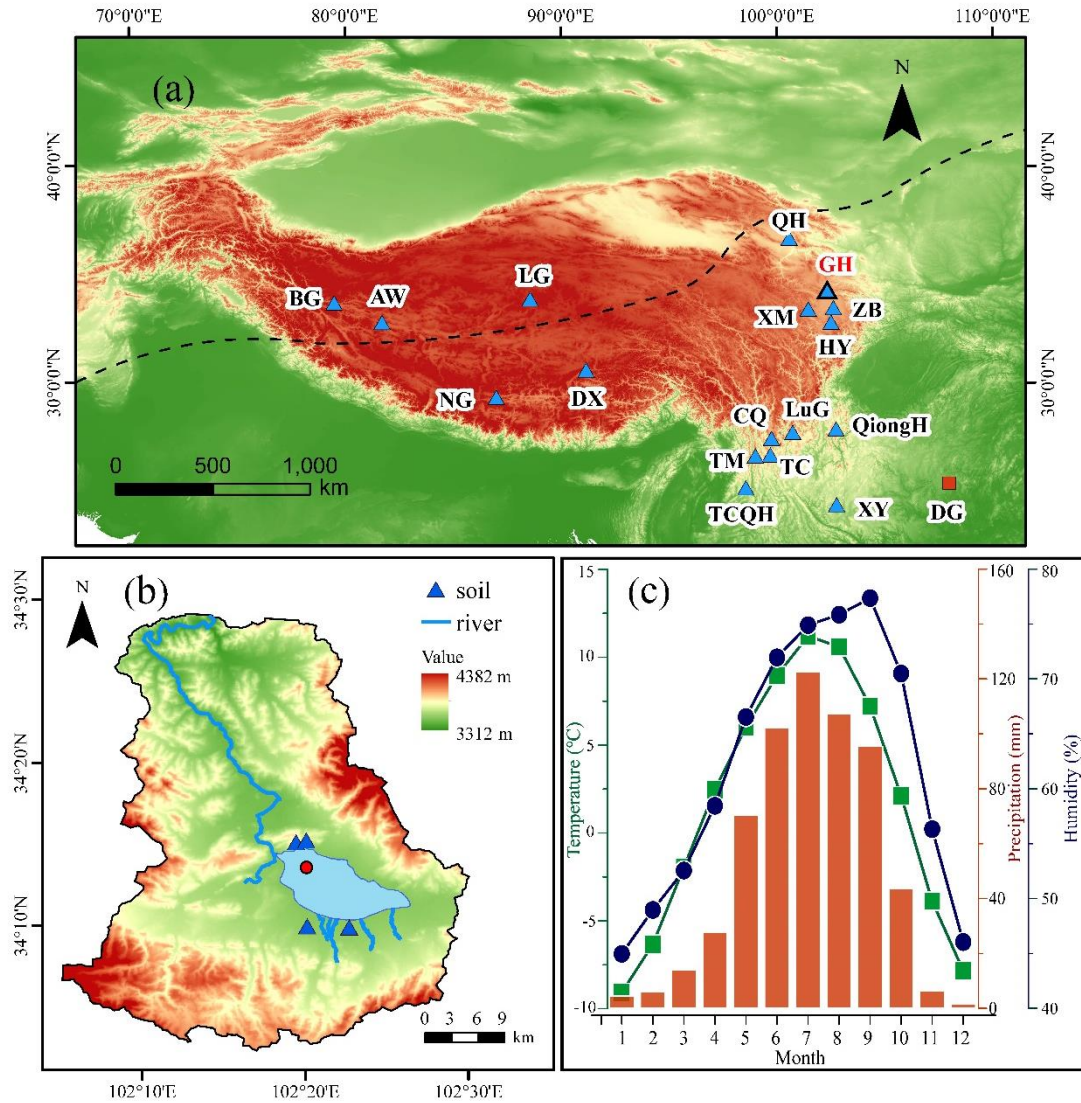
141 In this study, we obtained a quantitative temperature reconstruction for the past 15 ka from
142 Gahai, a shallow (average depth of ~2 m) freshwater lake located in the source area of the
143 Yellow River. This region is an important ecological protection area on the eastern edge of
144 the TP. Freshwater environments avoid the confounding effects of salinity on brGDGTs-
145 based temperature reconstructions, and shallow lakes also minimize the impact of the uneven

146 distribution of light and nutrients on brGDGTs. Our specific aims were: (1) to determine the
147 long-term trend of Holocene warm-biased terrestrial temperatures at a high elevation; (2) to
148 compare records of ice-free season temperatures with July temperatures from the same
149 sediment core; and (3) to gain a better understanding of the possible mechanisms responsible
150 for Holocene temperature variations, especially on the TP.

151 **2 Materials and methods**

152 *2.1 Study site*

153 Gahai (102°11'–102°28' E, 34°04'–34°4' N, 3444 m a.s.l.) is a freshwater lake and part of the
154 Gahai meadow wetland, which is a national nature reserve with restricted human access, on
155 the eastern edge of the Tibetan Plateau (Fig. 1). The lake is fed by runoff from the
156 surrounding hills, drains into the Tao River, and ultimately enters the Yellow River. Thus,
157 Gahai lake is a critical water conservation area in the upper reaches of the Yellow River. The
158 average water depth of Gahai is ~1–2 m, and the maximum depth is ~5 m. The vegetation in
159 the catchment consists mainly of *Kobresia tibetica*, *Equisetum arvense*, *Potentilla anserina*,
160 *Artemisia subulate*, and *Oxytropis falcata* (Ma et al., 2019). Meteorological data for the area
161 are available from Langmu Temple station (1957-1988) (Fig. 1) (102°38' E, 34°5' N, 3412 m
162 a.s.l.), ~32 km northwest of Gahai lake. They indicate an annual average (mean) precipitation
163 of 781 mm, with > 67% occurring between June and September, and mean annual
164 temperature of 1.2 °C with a relative humidity of ~65%. The summers are mild and humid
165 and the winters are cold and dry. From May to September, the mean average temperature is
166 above freezing (0°C), but the temperature in May is very low, close to 0°C.



167

168

169

170

171

172

173

174

175

176

177

178

Fig. 1 (a) Locations of the sites on the Tibetan Plateau referenced in the text. Triangle with bold line indicates the location of Gahai lake (this study). Other triangles indicate the locations of cited studies on the Tibetan Plateau and the surrounding area: Bangong Co (BG), Aweng Co (AW), Ngamring Co (NG), Linggo Co (LG), Dangxiong wetland (DX), Qinghai lake (QH), Ximen Co (XM), Zoige Basin (ZB), Hongyuan peatland (HY), Lugu lake (LuG), Cuoqia lake (CQ), Tingming lake (TM), Tengchongqinghai lake (TCQH), Tiancai lake (TC), Qionghai lake (QH), Xingyun lake (XY). Red square indicates Dongge Cave (DG). Black dotted line represents the northern boundary of the modern Asian summer Monsoon (Chen et al., 2008). (b) Drainage basin of Gahai lake and the core site. (c) Climate data from Langmu Temple meteorological station: monthly temperature (green line), precipitation (red bars), and humidity (blue line).

179 *2.2 Sampling*

180 A sediment core with the length of 329 cm was obtained from Gahai Lake in January 2019, at
181 a water depth of 1.95 m, using a UWITEC platform operated from the frozen lake surface. In
182 addition, four catchment soil samples were collected from around the lake (Fig. 1). All
183 samples were transported to the Institute of Tibetan Plateau Research, Chinese Academy of
184 Sciences (ITPCAS). The sediment core was split lengthwise, and one half was subsampled
185 and freeze-dried for subsequent analysis.

186

187 *2.3 Chronology*

188 The chronology of the upper 20 cm of the sediment core is based on measurements of ^{210}Pb
189 and ^{137}Cs , at a 1-cm interval. The chronology for the deeper part of the core is provided by
190 accelerator mass spectrometry (AMS) ^{14}C measurements of 13 bulk sediment samples, which
191 were conducted by Beta Analytic Inc. (Miami, USA) (Fig. 2) (Wang et al., 2022).

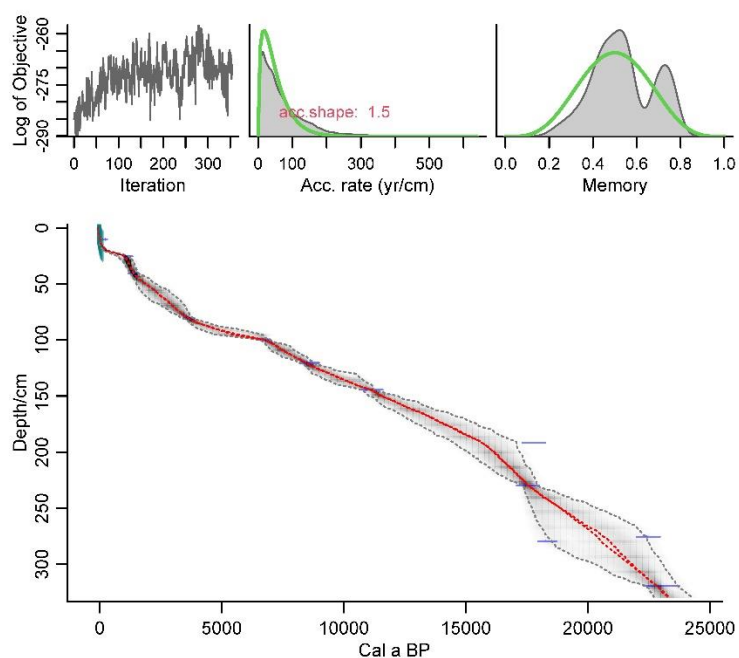
192

193 The ^{210}Pb age model was constructed using the constant rate of supply (CRS) model and the
194 ^{137}Cs peak was used as supplement (Appleby, 2002). The calculated age of ^{210}Pb using CRS
195 model aligned well with the ^{137}Cs peak at 6 cm. Overall, the CRS model was deemed suitable
196 for determining the age of Gahai lake.

197

198 Reservoir age, as highlighted by Hou et al. (2012), is a crucial factor affecting the age
199 determination of lake sediment cores on the TP. Therefore, it was necessary to establish the
200 reservoir age of Gahai lake before undertaking paleoclimate reconstruction. The linear

201 extrapolation relationship between the ^{14}C ages and depth to the sediment-water interface is
202 often used to estimate the reservoir age. The ^{14}C age of 13 samples exhibits a good linear
203 relationship with sediments depth in Gahai lake. Extrapolation of this 13 ^{14}C ages down to the
204 depth of 6 cm yielded a ^{14}C age of 461 yr BP, while the reliable ^{210}Pb age at 6 cm is -27 yr BP.
205 Consequently, the difference between the two ages, which amounts to 488 yr, was taken as
206 the reservoir age. Additionally, it's worth noting that independent estimations of the ^{14}C
207 calibration age and ^{210}Pb age around 10 cm in Gahai lake was obtained, resulting in values of
208 497 yr BP and 18 yr BP, respectively. The difference of 479 yr between these two ages can
209 also be considered as the reservoir age. These two methods of estimating reservoir age of
210 Gahai lake show very close, which are mutually supportive. So, the average of 483 yr was
211 adopted as the reservoir age. All original ^{14}C dates were corrected by subtracting the reservoir
212 age (483 yr) and calibrating them to calendar ages using Calib 8.1. The age-depth model (Fig.
213 2) was constructed using the Bacon program with the ^{14}C ages and ^{210}Pb ages (Blaauw and
214 Andres Christen, 2011) and was reported by Wang et al. (2022).



215

216 **Fig. 2** Age-depth model for Gahai, based on AMS ^{14}C , ^{210}Pb and ^{137}Cs ages (Wang et al.,
217 2022). The ages of the upper 20 cm are based on ^{210}Pb and ^{137}Cs dating (green symbols)
218 and those of the lower part on AMS ^{14}C dates (blue symbols).

219

220 *2.4 Lipids extraction and brGDGTs analysis*

221 For lipids extraction, ~5 g samples were ground to a powder and extracted ultrasonically with
222 dichloromethane (DCM): methanol (MeOH) (9: 1, v: v) three times. The supernatants were
223 combined and dried under a stream of nitrogen gas. Subsequently, the total lipid extracts were
224 separated into neutral and acid fractions through a LC-NH₂ silica gel column using DCM:
225 isopropyl alcohol (2: 1, v: v) and ether with 4% acetic acid (v: v), respectively. The neutral
226 fraction was then eluted through a silica gel column using n-Hexane, DCM and MeOH, and
227 the GDGTs were dissolved in the MeOH. The GDGTs fraction was passed through a 0.45 μm
228 polytetrafluoroethylene (PTFE) filter before analysis. C₄₆-GDGT (a standard compound)
229 (Huguet et al., 2006) was added to the samples before analysis.

230

231 BrGDGTs were detected using an HPLC-APCI-MS (Waters ACQUITY UPLC I-Class/Xevo
232 TQD) with auto-injection at the ITPCAS. The compounds were separated by three Hypersil
233 Gold Silica LC columns in sequence (each 100 mm \times 2.1 mm, 1.9 μm , Thermo Fisher
234 Scientific; USA), maintained at a temperature of 40°C. GDGTs were eluted isocratically
235 using 84% hexane and 16% ethyl acetate (EtOA) for the first 5 min, followed by a linear
236 gradient change to 82% hexane and 18% EtOA from 5 to 65 min. The columns were cleaned
237 using 100% EtOA for 10 min, and then back to 84% hexane and 16% EtOA to equilibrate the
238 column, with a flow rate of 0.2 ml min⁻¹.

239

240 The APCI-MS conditions were as follows: nebulizer pressure at 60 psi, APCI probe
241 temperature at 400°C, drying gas flow rate of 6 L/min and temperature of 200°C, capillary
242 voltage of 3600 V, source corona of 5.5 μ A. Detection was performed in selected ion
243 monitoring (SIM) mode, targeting the protonated molecules at m/z 1050, 1048, 1046, 1036,
244 1034, 1032, 1022, 1020, 1018 and 744. The results were analyzed using MassLynx V4.1
245 software, and quantification was achieved by comparing the peak areas of targeted ions and
246 the internal standard, assuming an identical response factor for GDGTs.

247

248 **3 Results and Discussion**

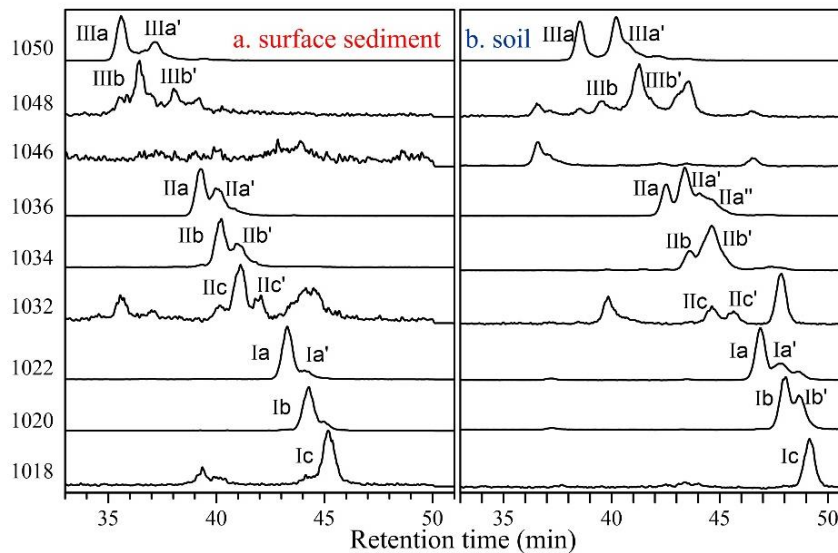
249 *3.1. Concentration and distribution of brGDGTs in the sediment core and catchment soils*

250 BrGDGTs were detected in both the catchment soils and the downcore sediments. The
251 average concentration of brGDGTs in the catchment soils (0.07 ng g⁻¹dw) was lower than in
252 the surficial core sediments (0.70 ng g⁻¹dw). In the soil samples, pentamethylated brGDGTs
253 were generally the most abundance (55.33%), followed by tetramethylated brGDGTs
254 (23.60%) and hexamethylated brGDGTs (21.07%) (Fig. S2). The relative amount of
255 cyclopentane ring-containing brGDGTs in the soil samples was generally low (24.34%) and it
256 was sometimes too low to be detected, especially the fractions of IIIb, IIIb', IIIc, IIIc', IIc and
257 IIc'. In the downcore sediments, the relative abundance of tetramethylated brGDGTs (43.84%)
258 was like that of pentamethylated brGDGTs (41.93%), and hexamethylated brGDGTs were the
259 least abundance (14.22%) (Fig. S2). The relative abundant of cyclopentane ring-containing
260 brGDGTs in the downcore sediments (67.82%) was lower than that in the catchment soils.

261 *3.2 In situ production of brGDGTs in Gahai lake*

262 Although lacustrine brGDGTs have great potential for quantitatively reconstructing terrestrial
263 paleotemperatures, uncertainties about their sources in lacustrine environments are a major
264 factor limiting their application (Buckles et al., 2014; Cao et al., 2020; Sinninghe Damsté et
265 al., 2009; Sun et al., 2011; Tierney and Russell, 2009). To investigate the origin and
266 characteristics of brGDGTs in the Gahai lake sediments, we examined the distributions and
267 concentrations of brGDGTs in the sediments and catchment soils and found notable
268 differences between them. First, as described in the previous section, the average content of
269 brGDGTs in the catchment soils was ~10% that of the surficial lake sediments, suggesting the
270 absence of large-scale allochthonous inputs from the catchment soils. Second, the brGDGTs
271 distributions in the downcore sediments were quite different from those in the catchment soils,
272 which suggests a substantial autochthonous brGDGTs contribution to the lake sediments (Fig.
273 3 and Fig. S2). Moreover, the ratios of 6-methyl brGDGTs to 5-methyl GDGTs (IR_{6ME}) in the
274 soils and sediments, calculated according to the formula proposed by De Jonge et al. (2014),
275 were different. In the soil samples, IR_{6ME} varied between 0.54 and 0.57 and the average ratio
276 in the downcore samples was 0.26, varying between 0.18 and 0.47. Third, the in-situ
277 production of brGDGTs in Gahai lake is suggested by the discrepancies in the degree of
278 methylation (MBT'_{5ME}) between the soils and surface sediments. The average value of
279 MBT'_{5ME} in the Gahai lake surface sediments was 0.48, which is clearly higher than in the
280 catchment soils, with the range of 0.32–0.35. Fourth, and potentially the most significant, the
281 IIIb' and Ib' compounds are present in the catchments soil but not in the Gahai lake surficial
282 sediments, which may be direct evidence of an autochthonous brGDGTs contribution in the

283 lacustrine environment (Fig. 3), and a lower proportion of soil-derived brGDGTs input.
 284 Therefore, we conclude that the brGDGTs in the Gahai lake sediments are mainly of in-situ
 285 origin.



286

287 **Fig. 3** Representative high-performance liquid chromatography/atmospheric pressure
 288 chemical ionization-mass spectrometry (HPLC/APCIMS) chromatograms of brGDGTs
 289 from (a) surface sediments from Gahai lake, and (b) soils in the catchment of Gahai lake.

290

291 3.3 brGDGTs-temperature calibration and Holocene temperature reconstruction

292 Gahai is a shallow lake in the eastern Tibetan Plateau that is typically completely frozen
 293 during winter and spring. Local meteorological data indicate that the average snowfall period
 294 lasts for 269 days, with around 50 days of continuous snowfall (Luqu County Local
 295 Chronicles Compilation Committee, 2006). The freezing of the lake surface begins in late
 296 October each year and gradually thaws starting from May of the following year. As a result,
 297 the light transmittance and oxygen content in the lake water are reduced during the freezing
 298 season, leading to decreased nutrient levels, which severely hinder the growth of autotrophic

299 microorganisms. Although the bacteria responsible for producing brGDGTs have not been
300 thoroughly characterized, the abundance of heterotrophic bacteria will likely decrease due to
301 the reduced autotrophic biomass during the winter and spring ice-covered period. The
302 weakened light penetration, decreased oxygen levels, and lack of nutrient replenishment
303 during the frozen period significantly impact the growth of autochthonous microorganisms.

304

305 While the specific bacterial species responsible for brGDGT production are not yet well
306 understood, it is known that these bacteria, as heterotrophic organisms, will also be
307 influenced by the reduction in autotrophic biomass. Furthermore, some research suggests that
308 the production of brGDGTs might be related to factors such as water depth, seasonal
309 alternation of water column mixing and stratification (Loomis et al., 2014; van Bree et al.,
310 2020). During the summer and autumn seasons when the lake ice melts and the water
311 becomes more mobile, the nutrient content increases, resulting in elevated lake biomass,
312 moreover, the oxygen levels at the bottom of Gahai lake are not expected to be too high,
313 which could further contribute to the proliferation of brGDGT-producing bacteria, potentially
314 leading to an increase in the brGDGT-producing bacteria (Weber et al., 2018). Therefore,
315 brGDGTs in Gahai lake may provide records of the average temperature during the ice-free
316 months of the summer and autumn seasons.

317

318 Additionally, the presence of the frozen lake surface during winter creates a thermal barrier,
319 impeding the exchange of heat between the lake water and the atmosphere. Consequently,
320 any brGDGTs generated within the lake water during this period lose their ability to

321 accurately reflect atmospheric temperature variations (Sun et al., 2021; Zhang et al., 2022a).
322 Thus, they were no longer able to track atmospheric temperature changes during the frozen
323 season. So, we prefer to use Gahai brGDGTs to reconstruct temperatures during the summer
324 and ice-free seasons. For this purpose, we employed the new Bayesian calibration for the
325 mean temperature of the Months Above Freezing, as proposed by Martínez-Sosa et al. (2021),
326 to derive a warm-biased temperature for Gahai lake.

327

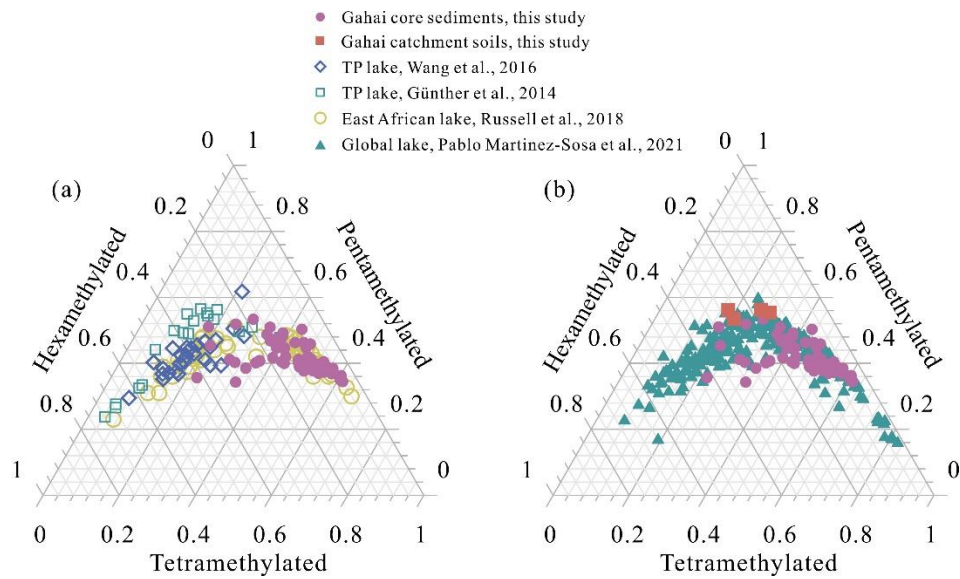
328 To assess the accuracy of this calibration approach, we compared the fractional abundances
329 of summed tetra-, penta-, and hexamethylated brGDGTs in Gahai lake sediments with other
330 datasets (Fig. 4). These datasets include lake sediments from the Tibetan Plateau (Günther et
331 al., 2014; Wang et al., 2016), East Africa (Russell et al., 2018), and global lakes (Martínez-
332 Sosa et al., 2021). The distribution pattern of Gahai core sediments is distinctly remarkable
333 compared to that of other lake sediments within the Tibetan Plateau, even though they share a
334 common regional origin (Fig. 4). However, its resemblance to the global distribution of
335 brGDGTs in lake sediments is evident. Notably, the calibration developed by Martínez-Sosa
336 et al. (2021) is based on brGDGTs from a global lake dataset.

337

338 Using calibration of Martínez-Sosa's et al. (2021), we reconstructed the surface sediment
339 temperature of Gahai lake, resulting in a temperature estimate of 9.4°C. This reconstructed
340 temperature closely matches the ice-free season temperature recorded by meteorological
341 stations in the Gahai region (8.8°C for May to September). Furthermore, considering the
342 significant contribution of autochthonous brGDGTs in Gahai lake, we also attempted to

343 reconstruct the Holocene paleotemperature record using previously published lake-specific
344 brGDGTs-temperature calibrations (e.g., Dang et al., 2018; Günther et al., 2014; Martínez-
345 Sosa et al., 2021; Russell et al., 2018; Sun et al., 2011; Wang et al., 2016). As illustrated in
346 Fig. S3, most of these calibrations showed qualitatively similar patterns of temperature
347 change when applied to the sediment core from Gahai lake. However, the magnitudes of
348 temperature fluctuations varied considerably and were found to be unsuitable for application
349 in Gahai lake due to several key reasons. Firstly, the fractional abundances of summed tetra-,
350 penta-, and hexamethylated brGDGTs in Gahai lake were inconsistent with those found in the
351 reference datasets (Fig. 4). Secondly, the analytical technique used for distinguishing 5- and
352 6-methyl isomers, which was a crucial aspect of some calibration studies (Günther et al.,
353 2014; Wang et al., 2016), was not employed in those studies, resulting in their exclusion from
354 our analysis. Thirdly, although the brGDGTs fractions in Gahai lake are resembled those of
355 East African lakes, the annual mean temperature reconstructed using this calibration
356 significantly differed from the temperature data recorded at the Langmu Temple station.
357 Moreover, even though the paleotemperature reconstruction for Gahai lake based on the
358 warm-season temperature calibration by Dang et al. (2018) showed similarity to the
359 calibration by Martínez-Sosa et al. (2021). However, it is worth noting that the calibration by
360 Dang et al. (2018) was established based on an investigation of 35 Chinese alkaline lakes,
361 which may not be directly applicable to the freshwater environment of Gahai lake. Similarly,
362 despite the salinity correction, the calibration reported by Wang et al. (2021) was not
363 considered suitable for our study.

364



365

366 **Fig. 4** Comparison of the fractional abundances of tetramethylated, pentamethylated, and
 367 hexamethylated bGDGTs in sediment core samples from Gahai with lake surface
 368 sediments from the Tibetan Plateau (Günther et al., 2014; Wang et al., 2016), East Africa
 369 (Russell et al., 2018), and worldwide (Martínez-Sosa et al., 2021).

370 Given these limitations, we ultimately opted to use the new Bayesian calibration for the mean
 371 temperature of the Months Above Freezing, as proposed by Martínez-Sosa et al. (2021), to
 372 reconstruct a warm-biased temperature record for Gahai lake.

373

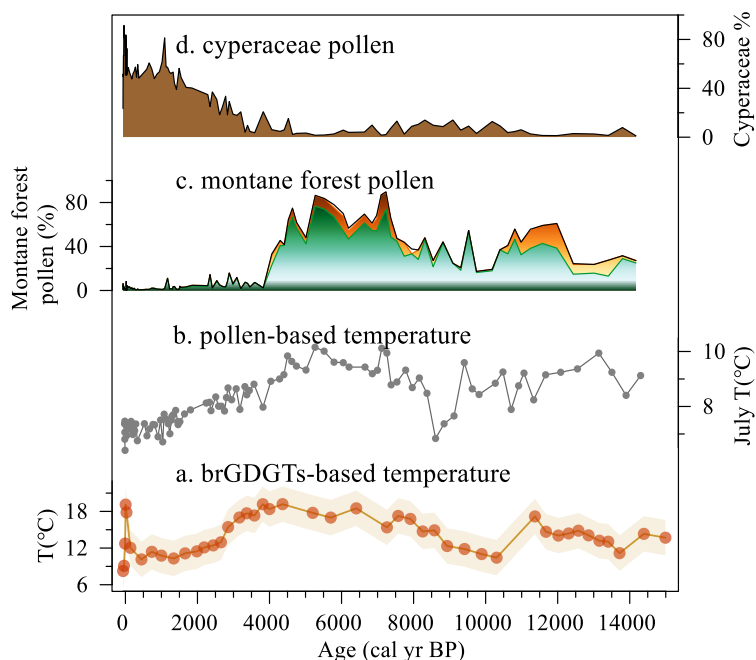
374 The depth interval of 191–279 cm in the Gahai sediment core represents an interval of rapid
 375 allocthonous sedimentation, or alternatively a slump, and therefore the results for the
 376 corresponding time interval of 20–15 ka may be unreliable. Thus, our temperature record of
 377 Months Above Freezing from the eastern TP spans the past 15 ka, with the average
 378 temperature of 4°C, as shown in Fig. 5a. Within the range of age uncertainties, weak warming
 379 occurred during 14.8–11.8 ka, likely to corresponding to the Bølling–Allerød (B/A)
 380 interstadial. A minor cold reversal occurred during 11.8–10.5 ka, potentially corresponding to
 381 the Younger Dryas (YD) event. Notably, the samples collected between 11.8 ka and 10.5 ka

382 exhibited GDGT concentrations below the detection limit. Therefore, we directly linked the
383 temperature reconstructions at the two aforementioned time points, ~11.8 ka and ~10.5 ka,
384 resulting in the lowest temperature of this time period appearing around 10.5 ka. This may
385 cause a time lag with the occurrence of the YD event. The temperature record indicates a
386 colder period during 11.5–8.0 ka. During 8.0–3.5 ka, Gahai experienced a stable warm period
387 with the average temperature of ~16.5°C, after which the temperature decreased gradually.
388 Overall, the maximum temperature difference since 15 ka was ~10°C. As for the absolute
389 temperature changes since 15,000 yr, although some influential studies indicate a warming of
390 approximately 6.1-7°C from the deglaciation onset to preindustrial times (Osman et al., 2021;
391 Tierney et al., 2020). However, these results are based on global mean sea surface
392 temperatures. Our reconstructed temperature range is about 10°C, considering the remarkable
393 ‘elevation-dependent warming’ observed in high-altitude regions compared to low-altitude
394 areas (Mountain Initiative EDW Working Group, 2015). Thus, this range could be accurate.
395 Nevertheless, we do not rule out the possibility that our temperature reconstruction may
396 exhibit an overestimation. This is a known issue in temperature reconstruction using
397 biomarkers. Aside from potential uncertainties associated with the biomarkers themselves,
398 calibrations may also considerably influence the observed amplitude. We examined
399 temperature variations reconstructed using different calibrations (Fig. S3), with the smallest
400 range being 6°C and the largest being 12°C. Undoubtedly, further efforts are needed to
401 constrain the inherent uncertainties related to biomarker-based temperature reconstructions.

402

403 *3.4 Holocene temperature changes on the eastern edge of TP and their origin*

404 Despite the difference in amplitude, the temperature record of Months Above Freezing from
 405 Gahai resembles the pollen record and the pollen-based temperature reconstruction from the
 406 same site (Fig. 5) (Wang et al., 2022). However, the brGDGTs-based Holocene Thermal
 407 Maximum (HTM) lags the pollen-based reconstruction (Fig. 5a, b). Wang et al. (2022) used a
 408 weighted-averaging partial least regression approach to produce a temperature record for
 409 Gahai, based on a modern pollen dataset (n=731) from the eastern TP. Assessment of the
 410 statistical significance of the pollen-based climate variables for Gahai suggests that the mean
 411 July temperature is the most important environmental factor influencing the fossil pollen
 412 assemblages. The brGDGTs in Gahai are indicative of summer and autumn temperatures, and
 413 the mismatch between the temperature records inferred from brGDGTs and the pollen record
 414 may be attributed to the difference between the solar irradiance during June–October and that
 415 during July. A detailed analysis of this topic will be undertaken in the subsequent section.

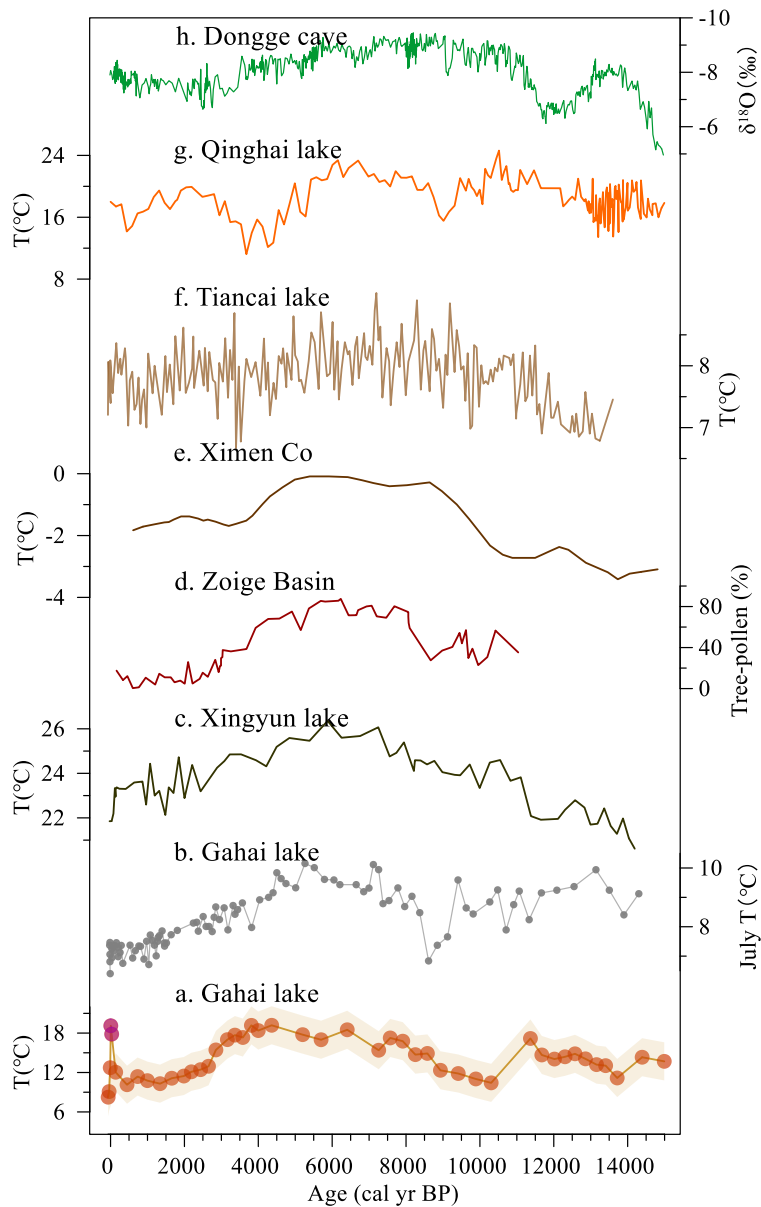


416
 417 **Fig. 5** Comparison of multiproxy records from Gahai lake. (a) brGDGTs-based warm-bias
 418 temperature (this study). (b) Temperature of the warmest month (July) based on pollen

419 assemblages (Wang et al., 2022). (c, d) Pollen-reconstructed montane forest (*Pinus*,
420 *Picea*, *Abies*) and Cyperaceae pollen record (Wang et al., 2022).

421

422 The brGDGTs-based temperature record from Gahai confirms the occurrence of a climate
423 optimum in the mid-Holocene on the northeast Tibetan Plateau, which is consistent with
424 several other pollen and pollen-reconstructed temperature records from the fringe areas of the
425 Asian summer monsoon (Fig. 6), suggesting that it is a reliable representation of Holocene
426 temperature changes in this region. For example, pollen-based temperature reconstructions
427 from Xingyun lake and Ximen Co on the eastern TP show a early to middle HTM (9–4 ka)
428 and a cooling trend thereafter (Fig. 6c, e) (Herzschuh et al., 2014; Wang et al., 2021a; Wu et
429 al., 2018). Additionally, lake water temperature reconstructions based on subfossil
430 chironomids from Tiancai lake (Fig. 6f) (Zhang et al., 2017; Zhang et al., 2019a) and
431 alkenones from Qinghai lake (Fig. 6g) (Hou et al., 2016) show the same trends during the
432 past 15 ka, as also shown by other pollen-based temperature records from the TP (Chen et al.,
433 2020). Pollen, chironomids and alkenones mainly respond to the growing season
434 temperatures in middle and high latitudes, and thus the reconstructed temperature records are
435 consistent with the variations in summer solar irradiance. Similar variations were documented
436 in temperature reconstructions at a global scale (Cartapanis et al., 2022; Marcott et al., 2013).

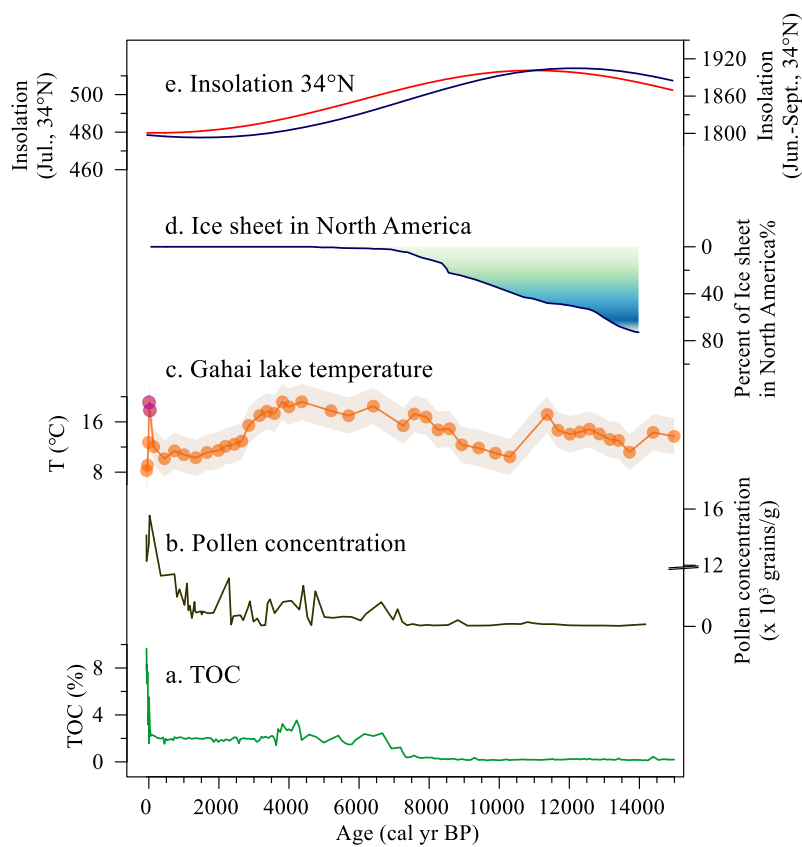


437

438 **Fig. 6** Comparison of temperature at Gahai and other records from the eastern edge of the
 439 Tibetan Plateau. (a) brGDGTs-based warm-bias temperature at Gahai, the purple dots
 440 may indicate unreliable temperature changes influenced by human activities (this study).
 441 (b) Temperature of the warmest month (July) based on pollen data from Gahai (Wang et
 442 al., 2022). (c) Pollen-based temperature at Xingyun lake (Wu et al., 2018). (d) Tree
 443 pollen percentages from the Hongyuan peatland in the southern Zoige Basin (Zhou et al.,
 444 2010). (e) Pollen-based temperature at Ximen Co (Herzschuh et al., 2014). (f)
 445 Chironomid-based temperature at Tiancai lake (Zhang et al., 2017, 2019a). (g)
 446 Alkenone-based temperature at Qinghai lake (Hou et al., 2016). (h) Stalagmite $\delta^{18}\text{O}$
 447 record of Dongge cave (Dykoski et al., 2005).

448

449 Nevertheless, the timing and amplitude of the Gahai temperature fluctuations differ from
450 those of other temperature records from this region (Fig. 6). These discrepancies may be the
451 result of the chronological uncertainties of these records, and to differences in the seasonal
452 and spatial responses to climate forcing and feedbacks. The temperature records shown in Fig.
453 6 mostly refer to summer temperatures, which are primarily influenced by summer insolation.



454

455 **Fig. 7** Temperature fluctuations and forcing factors during the Holocene. (a, b) TOC content
456 and pollen concentrations from Gahai (Wang et al., 2022). (c) brGDGTs-based warm-
457 bias temperature from Gahai, the purple dots may indicate unreliable temperature
458 changes influenced by human activities (this study). (d) Percentage of the remnant
459 Laurentide ice sheet in North America relative to the Last Glacial Maximum (Dyke,
460 2004). (e) Local insolation at 34 °N during ice-free months (Laskar et al., 2004).

461

462 The temperature record in Gahai during the early Holocene fails to closely track the Northern
463 Hemisphere insolation trend, and there is also a time lag. The pollen-based temperature
464 record for Xingyun Lake in southwestern China also shows lower temperatures in the early
465 Holocene (Fig. 6c). The albedo effect caused by the increased cloud cover may be the reason
466 for the early Holocene decrease in summer temperatures (Wu et al., 2018). However, the
467 pollen record from Gahai indicates dry conditions during the early Holocene (Wang et al.,
468 2022), and cloud cover may not be the primary factor responsible for the low temperatures at
469 this time. The melting of Northern Hemisphere ice sheets during the early Holocene
470 weakened the Atlantic Meridional Overturning Circulation (AMOC) and potentially also the
471 global thermohaline circulation. This led to a reduction in the amount of heat transport by the
472 North Atlantic warm current to high-latitude regions, which resulted in the low temperatures
473 in middle to high latitudes of the Northern Hemisphere. The persistence of the Laurentide ice
474 sheet into the early Holocene maintained the regional albedo, as well as discharging
475 meltwater into the North Atlantic (Fig. 7d) (Dyke, 2004). In addition, a Holocene temperature
476 simulation showed that global warming was more pronounced when dust factors were
477 excluded from the simulation (Liu et al. (2018). The record of insoluble particles in the
478 Greenland GISP2 ice core indicates relatively high concentrations of atmospheric aerosols in
479 the early Holocene (Zielinski and Mershon, 1997), which would have weakened summer
480 solar irradiation via radiative feedback, leading to the cool temperatures during this period.
481 These factors may together have caused the early Holocene temperature decline at Gahai
482 Lake, which slightly delayed the onset of the Holocene Warm Period.

483

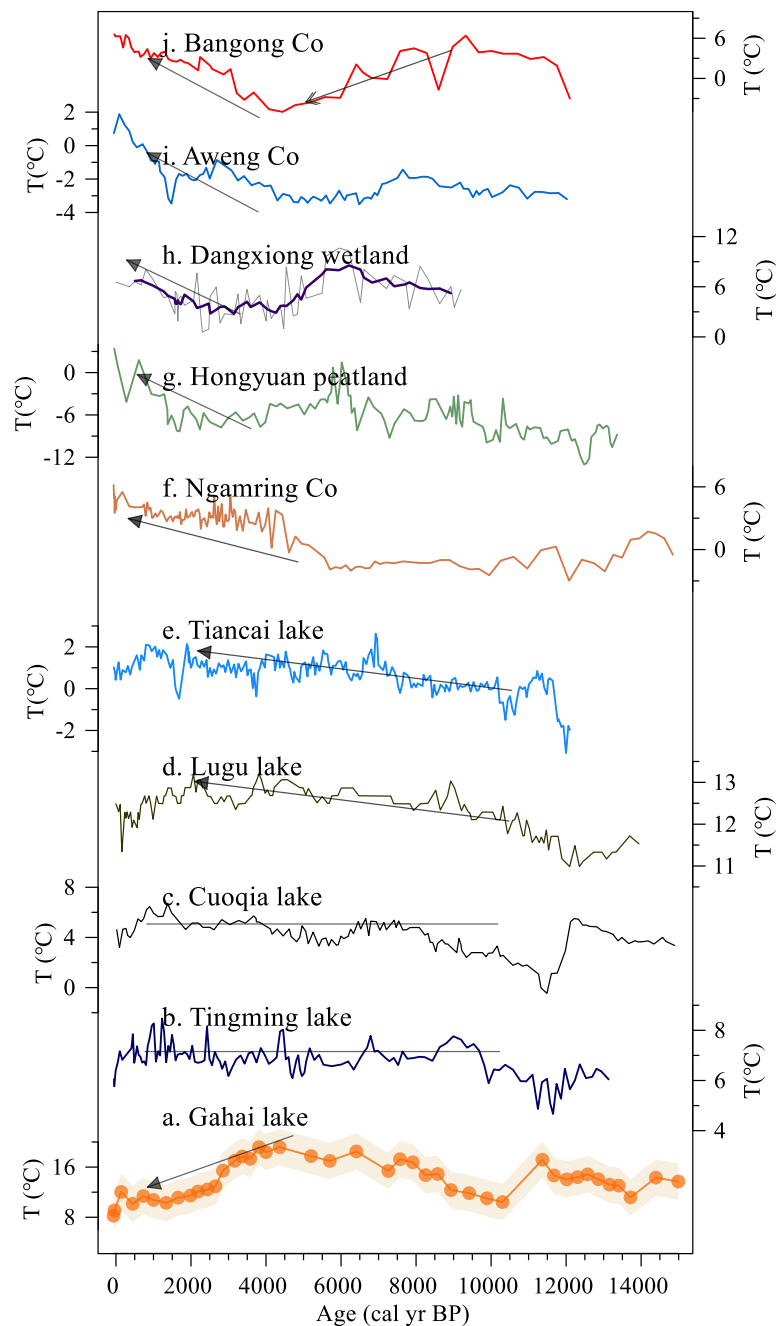
484 A notable and rapid temperature increase is evident at Gahai in recent decades, which differs
485 from the other records (Fig. 7c). Moreover, there are notable increases in pollen concentration,
486 TOC, and TN (Fig. 7a, b) in the Gahai sediment core, indicating intensive local human
487 activities like grazing and tourism, which may be the primary cause of the environmental
488 changes in this region (Wang et al., 2022). This intensive human activity may have reduced
489 the ability of the brGDGTs to record the natural temperature background. These observations
490 emphasize the important impact of human activities on climate proxies and the need to
491 carefully consider their effect on temperature reconstructions.

492

493 *3.5 Spatiotemporal pattern of brGDGTs-based TP temperatures*

494 In addition to comparing the Gahai temperature with the summer temperature records from
495 the eastern TP and its surrounding areas, we compiled and reviewed published Holocene
496 brGDGTs-based quantitative temperature records from across the TP. As shown in Fig. 8,
497 with the increasing number of these records for the TP, the differences between the results
498 have become more pronounced. The brGDGTs records from lakes in the central and western
499 parts of the plateau show higher temperatures in the early and late Holocene, and lower
500 temperatures in the middle Holocene (He et al., 2020; Li et al., 2017; Wang et al., 2021c),
501 while the brGDGTs records from lakes in the southern and south-eastern parts of the TP show
502 a warming trend throughout the Holocene (Feng et al., 2022; Sun et al., 2022). In addition,
503 brGDGTs in Cuoqia lake and Tingming lake, on the south-eastern TP, recorded the ice-free
504 season temperature, which was relatively stable during the Holocene (Sun et al., 2021; Zhang

505 et al., 2022a). However, our temperature record from Gahai is different from the above
 506 records and resembles summer temperature changes during the Holocene (Chen et al., 2020).
 507 This is because the brGDGTs record from Lake Gahai represents warm season temperatures,
 508 which adds to its reliability.



509
 510 **Fig. 8** Comparison of Holocene temperature based on brGDGTs at Gahai (a) and other
 511 records from around the TP. Reconstructed ice-free-season temperatures from (b)

512 Tingming lake (Sun et al., 2021), (c) Cuoqia lake (Zhang et al., 2022a). Reconstructed
513 annual temperature from (d) Lugu lake (Zhao et al., 2021b), (e) Tiancai lake (Feng et al.,
514 2022), (f) Ngamring Co(Sun et al., 2022), (g) Hongyuan peatland (Yan et al., 2021). (h)
515 Dangxiong wetland (Cheung et al., 2017), (i) Aweng Co (Li et al., 2017), (j) Bangong
516 Co (Wang et al., 2021c).

517

518 We suggest that the complexity of Holocene temperature patterns recorded by brGDGTs in
519 TP lakes is primarily due to the ambiguity of brGDGTs in these lakes, as well as to the spatial
520 heterogeneity of climate change across the TP. This ambiguity can be attributed to several
521 factors. First, the origin of brGDGTs in lakes remains an uncertain factor in temperature
522 reconstruction. An increasing number of studies indicate the occurrence of a remarkable
523 amount of autochthonous brGDGTs in lakes, but their abundance in soil can also affect the
524 distribution of brGDGTs in lakes due to their supply via soil erosion (e.g., Tierney and
525 Russell, 2009; Wang et al., 2023; Weber et al., 2015). In fact, even within the same lake (e.g.,
526 Tengchongqinghai lake in southwestern China), two studies reached inconsistent conclusions
527 regarding the origin of brGDGTs (Tian et al., 2019; Zhao et al., 2021b), possibly because the
528 niches of certain brGDGTs may expand or contract compared to other locations within a lake.
529 Therefore, it is important to conduct detailed modern process studies to accurately assess the
530 sources of brGDGTs in lakes, especially with regard to evaluating the proportion of
531 autochthonous brGDGTs (Martin et al., 2020; Wang et al., 2023). Second, brGDGTs may
532 show a seasonal signal. Current brGDGTs–temperature calibrations for lakes reflect the
533 annual average temperature (De Jonge et al., 2014; Sun et al., 2011), as well as the growing

534 season temperature (Dang et al., 2018; Sun et al., 2011) and the ice-free season temperature
535 (Martínez-Sosa et al., 2021; Zhang et al., 2022a). Thus, there is no consensus regarding
536 whether the brGDGTs have a seasonal bias, and it is necessary to conduct continuous, high-
537 resolution seasonal investigations of lakes on the Tibetan Plateau to comprehensively
538 elucidate the seasonal characteristics of brGDGTs. This can enhance the accuracy of regional
539 temperature reconstruction and may help reconcile the complex temperature patterns
540 observed on the Tibetan Plateau. Third, the factors affecting the distribution of brGDGTs in
541 lakes are complex, including not only temperature, pH and salinity but also oxygen content,
542 water depth, and so on (Wang et al., 2021b; Wang et al., 2016). The distribution of brGDGTs
543 in lakes is significantly influenced by the hydrological and physical properties of the lakes,
544 and thus it is necessary to attain a more comprehensive understanding of the characteristics of
545 the lakes in the study area and their effects on brGDGTs. Fourth, different brGDGTs-
546 temperature calibrations may lead to markable differences in both the amplitude and trend of
547 temperature from the same dataset (Feng et al., 2019; Wang et al., 2016). One reason for this
548 is the deviation between in-situ measured temperature and atmospheric temperature (Wang et
549 al., 2020). Thus, selecting an appropriate calibration and attempting to establish a brGDGTs-
550 in situ temperature calibration are effective means of enhancing the reliability of brGDGTs-
551 based temperature reconstructions.

552

553 **4 Conclusions**

554 We present a quantitative, brGDGTs-based seasonal paleotemperature record over the last 15
555 ka from the sediments of a shallow lake on the eastern Tibetan Plateau. Our reconstruction

556 resembles the summer temperature trend, with the Holocene Thermal Maximum occurring
557 during 8–3.5 ka. There is a lag between our brGDGTs-based reconstruction and pollen-based
558 July temperature recorded in the same sediment core, indicating a seasonal bias between
559 different proxies. Since 3.5 ka, the temperature decreased gradually, and the surficial
560 sediments reliably recorded the warm season temperature during the current period in the
561 Gahai Lake region. However, intensive local human activity during the last century has
562 affected the distribution of brGDGTs, resulting in temperature deviations recorded by
563 brGDGTs. However, the implementation of environmental protection policies have reduced
564 this anthropogenic signal. Our findings help better understand the seasonal signal of
565 brGDGTs in shallow lakes and provide important data for improving projections of terrestrial
566 climate change at high elevations.

567

568 We also investigated previously published brGDGTs-based Holocene temperature records on
569 the TP to determine the pattern of brGDGTs-based temperature changes and the possible
570 causes of the differences between reconstructions. We emphasize the need for the careful
571 examination of both the source and behavior of these compounds in lacustrine environments
572 and lake status, prior to the application of brGDGTs proxies in paleolimnological
573 reconstruction.

574

575 **Competing interests**

576 The contact author has declared that none of the authors has any competing interests.

577

578 **Acknowledgements**

579 This work was financially supported by the National Natural Science Foundation of China
580 (42025103, 41877459) and the Second Tibetan Plateau Scientific Expedition and Research
581 (2019QZKK0601). We would like to thank Jan Bloemendal for the help with language
582 editing.
583

584 References

585

586 Bova, S., Rosenthal, Y., Liu, Z., Godad, S.P., Yan, M., 2021. Seasonal origin of the thermal
587 maxima at the Holocene and the last interglacial. *Nature* 589, 548-553.

588 Buckles, L.K., Weijers, J.W.H., Verschuren, D., Damste, J.S.S., 2014. Sources of core and
589 intact branched tetraether membrane lipids in the lacustrine environment: Anatomy of
590 Lake Challa and its catchment, equatorial East Africa. *Geochimica Et Cosmochimica*
591 *Acta* 140, 106-126.

592 Cao, J., Rao, Z., Shi, F., Jia, G., 2020. Ice formation on lake surfaces in winter causes warm-
593 season bias of lacustrine brGDGT temperature estimates. *Biogeosciences* 17, 2521-2536.

594 Cartapanis, O., Jonkers, L., Moffa-Sanchez, P., Jaccard, S.L., de Vernal, A., 2022. Complex
595 spatio-temporal structure of the Holocene Thermal Maximum. *Nat Commun* 13, 5662.

596 Chen, D., Xu, B., Yao, T., Guo, Z., Cui, P., Chen, F., Zhang, R., Zhang, X., Zhang, Y., Fan, J.,
597 Hou, Z., Zhang, T., 2015. Assessment of past, present and future environmental changes
598 on the Tibetan Plateau. *Chinese Science Bulletin* 60, 3025-3035.

599 Chen, F., Yu, Z., Yang, M., Ito, E., Wang, S., Madsen, D.B., Huang, X., Zhao, Y., Sato, T.,
600 Birks, H.J.B., Boomer, I., Chen, J., An, C., Wünnemann, B., 2008. Holocene moisture
601 evolution in arid central Asia and its out-of-phase relationship with Asian monsoon
602 history. *Quaternary Science Reviews* 27, 351-364.

603 Chen, F., Zhang, J., Liu, J., Cao, X., Hou, J., Zhu, L., Xu, X., Liu, X., Wang, M., Wu, D.,
604 Huang, L., Zeng, T., Zhang, S., Huang, W., Zhang, X., Yang, K., 2020. Climate change,
605 vegetation history, and landscape responses on the Tibetan Plateau during the Holocene:
606 A comprehensive review. *Quaternary Science Reviews* 243.

607 Chen, Y., Zheng, F., Yang, H., Yang, W., Wu, R., Liu, X., Liang, H., Chen, H., Pei, H., Zhang,
608 C., Pancost, R.D., Zeng, Z., 2022. The production of diverse brGDGTs by an
609 *Acidobacterium* providing a physiological basis for paleoclimate proxies. *Geochimica et*
610 *Cosmochimica Acta* 337, 155-165.

611 Cheung, M.-C., Zong, Y., Zheng, Z., Liu, Z., Aitchison, J.C., 2017. Holocene temperature and
612 precipitation variability on the central Tibetan Plateau revealed by multiple palaeo-
613 climatic proxy records from an alpine wetland sequence. *The Holocene* 27, 1669-1681.

614 Committee, L.C.L.C.C., 2006. Luqu County Chronicles. Gansu Cultural Publishing House,
615 Lanzhou.

616 Crampton-Flood, E.D., Tierney, J.E., Peterse, F., Kirkels, F.M.S.A., Damste, J.S.S., 2020.
617 BayMBT: A Bayesian calibration model for branched glycerol dialkyl glycerol
618 tetraethers in soils and peats. *Geochimica Et Cosmochimica Acta* 268, 142-159.

619 Dang, X., Ding, W., Yang, H., Pancost, R.D., Naafs, B.D.A., Xue, J., Lin, X., Lu, J., Xie, S.,
620 2018. Different temperature dependence of the bacterial brGDGT isomers in 35 Chinese
621 lake sediments compared to that in soils. *Organic Geochemistry* 119, 72-79.

622 De Jonge, C., Hopmans, E.C., Zell, C.I., Kim, J.-H., Schouten, S., Sinninghe Damsté, J.S.,
623 2014. Occurrence and abundance of 6-methyl branched glycerol dialkyl glycerol
624 tetraethers in soils: Implications for palaeoclimate reconstruction. *Geochimica et*
625 *Cosmochimica Acta* 141, 97-112.

626 Ding, S., Xu, Y., Wang, Y., He, Y., Hou, J., Chen, L., He, J.S., 2015. Distribution of branched
627 glycerol dialkyl glycerol tetraethers in surface soils of the Qinghai-Tibetan Plateau:

628 implications of brGDGTs-based proxies in cold and dry regions. *Biogeosciences* 12,
629 3141-3151.

630 Dong, Y., Wu, N., Li, F., Zhang, D., Zhang, Y., Shen, C., Lu, H., 2022. The Holocene
631 temperature conundrum answered by mollusk records from East Asia. *Nat Commun* 13,
632 5153.

633 Dyke, A.S., 2004. An outline of North American deglaciation with emphasis on central and
634 northern Canada. *Quaternary Glaciations-Extent and Chronology, Pt 2: North America* 2,
635 373-424.

636 Dykoski, C.A., Edwards, R.L., Cheng, H., Yuan, D.X., Cai, Y.J., Zhang, M.L., Lin, Y.S., Qing,
637 J.M., An, Z.S., Revenaugh, J., 2005. A high-resolution, absolute-dated Holocene and
638 deglacial Asian monsoon record from Dongge Cave, China. *Earth and Planetary Science*
639 *Letters* 233, 71-86.

640 Feng, X., Zhao, C., D'Andrea, W.J., Liang, J., Zhou, A., Shen, J., 2019. Temperature
641 fluctuations during the Common Era in subtropical southwestern China inferred from
642 brGDGTs in a remote alpine lake. *Earth and Planetary Science Letters* 510, 26-36.

643 Feng, X., Zhao, C., D'Andrea, W.J., Hou, J., Yang, X., Xiao, X., Shen, J., Duan, Y., Chen, F.,
644 2022. Evidence for a Relatively Warm Mid-to Late Holocene on the Southeastern
645 Tibetan Plateau. *Geophysical Research Letters* 49.

646 Group, M.I.E.W., 2015. Elevation-dependent warming in mountain regions of the world.
647 *Nature Climate Change* 5, 424-430.

648 Günther, F., Thiele, A., Gleixner, G., Xu, B., Yao, T., Schouten, S., 2014. Distribution of
649 bacterial and archaeal ether lipids in soils and surface sediments of Tibetan lakes:
650 Implications for GDGT-based proxies in saline high mountain lakes. *Organic*
651 *Geochemistry* 67, 19-30.

652 Halamka, T.A., Raberg, J.H., McFarlin, J.M., Younkin, A.D., Mulligan, C., Liu, X.L., Kopf,
653 S.H., 2022. Production of diverse brGDGTs by *Acidobacterium Solibacter usitatus* in
654 response to temperature, pH, and O₂ provides a culturing perspective on brGDGT
655 proxies and biosynthesis. *Geobiology*.

656 He, Y., Hou, J., Wang, M., Li, X., Liang, J., Xie, S., Jin, Y., 2020. Temperature Variation on
657 the Central Tibetan Plateau Revealed by Glycerol Dialkyl Glycerol Tetraethers From the
658 Sediment Record of Lake Linggo Co Since the Last Deglaciation. *Frontiers in Earth*
659 *Science* 8.

660 Herzschuh, U., Borkowski, J., Schewe, J., Mischke, S., Tian, F., 2014. Moisture-advection
661 feedback supports strong early-to-mid Holocene monsoon climate on the eastern Tibetan
662 Plateau as inferred from a pollen-based reconstruction. *Palaeogeography,*
663 *Palaeoclimatology, Palaeoecology* 402, 44-54.

664 Hou, J., Huang, Y., Zhao, J., Liu, Z., Colman, S., An, Z., 2016. Large Holocene summer
665 temperature oscillations and impact on the peopling of the northeastern Tibetan Plateau.
666 *Geophysical Research Letters* 43, 1323-1330.

667 Hou, J., Li, C., Lee, S., 2019. The temperature record of the Holocene: progress and
668 controversies. *Science Bulletin*.

669 Huguet, C., Hopmans, E.C., Febo-Ayala, W., Thompson, D.H., Sinninghe Damsté, J.S.,
670 Schouten, S., 2006. An improved method to determine the absolute abundance of
671 glycerol dibiphytanyl glycerol tetraether lipids. *Organic Geochemistry* 37, 1036-1041.

- 672 Kuang, X., Jiao, J.J., 2016. Review on climate change on the Tibetan Plateau during the last
673 half century. *Journal of Geophysical Research: Atmospheres* 121, 3979-4007.
- 674 Laskar, J., Robutel, P., Joutel, F., Gastineau, M., Correia, A.C.M., Levrard, B., 2004. A long-
675 term numerical solution for the insolation quantities of the Earth. *Astronomy &*
676 *Astrophysics* 428, 261-285.
- 677 Li, X., Wang, M., Zhang, Y., Lei, L., Hou, J., 2017. Holocene climatic and environmental
678 change on the western Tibetan Plateau revealed by glycerol dialkyl glycerol tetraethers
679 and leaf wax deuterium-to-hydrogen ratios at Aweng Co. *Quaternary Research* 87, 455-
680 467.
- 681 Liu, Y., Zhang, M., Liu, Z., Xia, Y., Huang, Y., Peng, Y., Zhu, J., 2018. A Possible Role of
682 Dust in Resolving the Holocene Temperature Conundrum. *Scientific Reports* 8.
- 683 Liu, Z.Y., Zhu, J., Rosenthal, Y., Zhang, X., Otto-Bliesner, B.L., Timmermann, A., Smith,
684 R.S., Lohmann, G., Zheng, W.P., Timm, O.E., 2014. The Holocene temperature
685 conundrum. *Proc. Natl. Acad. Sci. U. S. A.* 111, E3501-E3505.
- 686 Loomis, S.E., Russell, J.M., Heuroux, A.M., D'Andrea, W.J., Sinninghe Damsté, J.S., 2014.
687 Seasonal variability of branched glycerol dialkyl glycerol tetraethers (brGDGTs) in a
688 temperate lake system. *Geochimica et Cosmochimica Acta* 144, 173-187.
- 689 Lu, H., Wu, N., Liu, K.-b., Zhu, L., Yang, X., Yao, T., Wang, L., Li, Q., Liu, X., Shen, C., Li,
690 X., Tong, G., Jiang, H., 2011. Modern pollen distributions in Qinghai-Tibetan Plateau
691 and the development of transfer functions for reconstructing Holocene environmental
692 changes. *Quaternary Science Reviews* 30, 947-966.
- 693 Ma, W., Li, G., Song, J., Yan, L., Wu, L., 2019. Effect of Vegetation Degradation on Soil
694 Organic Carbon Pool and Carbon Pool Management Index in the Gahai Wetland, China.
695 *Acta Agrestia Sinica* 27, 687-694.
- 696 Marcott, S.A., Shakun, J.D., Clark, P.U., Mix, A.C., 2013. A Reconstruction of Regional and
697 Global Temperature for the Past 11,300 Years. *Science* 339, 1198-1201.
- 698 Marsicek, J., Shuman, B.N., Bartlein, P.J., Shafer, S.L., Brewer, S., 2018. Reconciling
699 divergent trends and millennial variations in Holocene temperatures. *Nature* 554, 92-+.
- 700 Martin, C., Ménot, G., Thouveny, N., Peyron, O., Andrieu-Ponel, V., Montade, V., Davtian,
701 N., Reille, M., Bard, E., 2020. Early Holocene Thermal Maximum recorded by branched
702 tetraethers and pollen in Western Europe (Massif Central, France). *Quaternary Science*
703 *Reviews* 228, 106109.
- 704 Martínez-Sosa, P., Tierney, J.E., Stefanescu, I.C., Dearing Crampton-Flood, E., Shuman, B.N.,
705 Routson, C., 2021. A global Bayesian temperature calibration for lacustrine brGDGTs.
706 *Geochimica et Cosmochimica Acta* 305, 87-105.
- 707 Moser, K.A., Baron, J.S., Brahney, J., Oleksy, I.A., Saros, J.E., Hundey, E.J., Sadro, S.,
708 Kopáček, J., Sommaruga, R., Kainz, M.J., Strecker, A.L., Chandra, S., Walters, D.M.,
709 Preston, D.L., Michelutti, N., Lepori, F., Spaulding, S.A., Christianson, K.R., Melack,
710 J.M., Smol, J.P., 2019. Mountain lakes: Eyes on global environmental change. *Global*
711 *and Planetary Change* 178, 77-95.
- 712 Opitz, S., Zhang, C., Herzschuh, U., Mischke, S., 2015. Climate variability on the south-
713 eastern Tibetan Plateau since the Lateglacial based on a multiproxy approach from Lake
714 Naleng – comparing pollen and non-pollen signals. *Quaternary Science Reviews* 115,
715 112-122.

- 716 Osman, M.B., Tierney, J.E., Zhu, J., Tardif, R., Hakim, G.J., King, J., Poulsen, C.J., 2021.
717 Globally resolved surface temperatures since the Last Glacial Maximum. *Nature* 599,
718 239-244.
- 719 Pang, H., Hou, S., Zhang, W., Wu, S., Jenk, T.M., Schwikowski, M., Jouzel, J., 2020.
720 Temperature Trends in the Northwestern Tibetan Plateau Constrained by Ice Core Water
721 Isotopes Over the Past 7,000 Years. *Journal of Geophysical Research-Atmospheres* 125.
- 722 Qiu, J., 2008. The third pole. *Nature* 454, 393-396.
- 723 Russell, J.M., Hopmans, E.C., Loomis, S.E., Liang, J., Sinninghe Damsté, J.S., 2018.
724 Distributions of 5- and 6-methyl branched glycerol dialkyl glycerol tetraethers
725 (brGDGTs) in East African lake sediment: Effects of temperature, pH, and new
726 lacustrine paleotemperature calibrations. *Organic Geochemistry* 117, 56-69.
- 727 Sinninghe Damsté, J.S., Hopmans, E.C., Pancost, R.D., Schouten, S., Geenevasen, J.A.J.,
728 2000. Newly discovered non-isoprenoid glycerol dialkyl glycerol tetraether lipids in
729 sediments. *Chemical Communications*, 1683-1684.
- 730 Sinninghe Damsté, J.S., Ossebaar, J., Abbas, B., Schouten, S., Verschuren, D., 2009. Fluxes
731 and distribution of tetraether lipids in an equatorial African lake: Constraints on the
732 application of the TEX86 palaeothermometer and BIT index in lacustrine settings.
733 *Geochimica et Cosmochimica Acta* 73, 4232-4249.
- 734 Sun, Q., Chu, G., Liu, M., Xie, M., Li, S., Ling, Y., Wang, X., Shi, L., Jia, G., Lü, H., 2011.
735 Distributions and temperature dependence of branched glycerol dialkyl glycerol
736 tetraethers in recent lacustrine sediments from China and Nepal. *Journal of Geophysical
737 Research* 116.
- 738 Sun, X., Zhao, C., Zhang, C., Feng, X., Yan, T., Yang, X., Shen, J., 2021. Seasonality in
739 Holocene Temperature Reconstructions in Southwestern China. *Paleoceanography and
740 Paleoclimatology* 36.
- 741 Sun, Z., Hou, X., Ji, K., Yuan, K., Li, C., Wang, M., Hou, J., 2022. Potential winter-season
742 bias of annual temperature variations in monsoonal Tibetan Plateau since the last
743 deglaciation. *Quaternary Science Reviews* 292.
- 744 Thompson, L.G., Yao, T., Davis, M.E., Henderson, K.A., MosleyThompson, E., Lin, P.N.,
745 Beer, J., Synal, H.A., ColeDai, J., Bolzan, J.F., 1997. Tropical climate instability: The
746 last glacial cycle from a Qinghai-Tibetan ice core. *Science* 276, 1821-1825.
- 747 Tian, L., Wang, M., Zhang, X., Yang, X., Zong, Y., Jia, G., Zheng, Z., Man, M., 2019.
748 Synchronous change of temperature and moisture over the past 50 ka in subtropical
749 southwest China as indicated by biomarker records in a crater lake. *Quaternary Science
750 Reviews* 212, 121-134.
- 751 Tierney, J.E., Russell, J.M., 2009. Distributions of branched GDGTs in a tropical lake system:
752 Implications for lacustrine application of the MBT/CBT paleoproxy. *Organic
753 Geochemistry* 40, 1032-1036.
- 754 Tierney, J.E., Russell, J.M., Eggermont, H., Hopmans, E.C., Verschuren, D., Sinninghe
755 Damsté, J.S., 2010. Environmental controls on branched tetraether lipid distributions in
756 tropical East African lake sediments. *Geochimica et Cosmochimica Acta* 74, 4902-4918.
- 757 Tierney, J.E., Zhu, J., King, J., Malevich, S.B., Hakim, G.J., Poulsen, C.J., 2020. Glacial
758 cooling and climate sensitivity revisited. *Nature* 584, 569-+.
- 759 van Bree, L.G.J., Peterse, F., Baxter, A.J., De Crop, W., van Grinsven, S., Villanueva, L.,

760 Verschuren, D., Sinninghe Damsté, J.S., 2020. Seasonal variability and sources of in situ
761 brGDGT production in a permanently stratified African crater lake. *Biogeosciences* 17,
762 5443-5463.

763 Wang, G., Wang, Y., Wei, Z., He, W., Ma, X., Zhang, T., 2021a. Reconstruction of
764 temperature and precipitation spanning the past 28 kyr based on branched tetraether
765 lipids from Qionghai Lake, southwestern China. *Palaeogeography Palaeoclimatology*
766 *Palaeoecology* 562.

767 Wang, H., An, Z., Lu, H., Zhao, Z., Liu, W., 2020. Calibrating bacterial tetraether
768 distributions towards in situ soil temperature and application to a loess-paleosol
769 sequence. *Quaternary Science Reviews* 231.

770 Wang, H., Liu, W., He, Y., Zhou, A., Zhao, H., Liu, H., Cao, Y., Hu, J., Meng, B., Jiang, J.,
771 Kolpakova, M., Krivonogov, S., Liu, Z., 2021b. Salinity-controlled isomerization of
772 lacustrine brGDGTs impacts the associated MBT5ME' terrestrial temperature index.
773 *Geochimica et Cosmochimica Acta* 305, 33-48.

774 Wang, H., Chen, W., Zhao, H., Cao, Y., Hu, J., Zhao, Z., Cai, Z., Wu, S., Liu, Z., Liu, W.,
775 2023. Biomarker-based quantitative constraints on maximal soil-derived brGDGTs in
776 modern lake sediments. *Earth and Planetary Science Letters* 602.

777 Wang, M., Liang, J., Hou, J., Hu, L., 2016. Distribution of GDGTs in lake surface sediments
778 on the Tibetan Plateau and its influencing factors. *Science China Earth Sciences* 59, 961-
779 974.

780 Wang, M.D., Hou, J.Z., Duan, Y.W., Chen, J.H., Li, X.M., He, Y., Lee, S.Y., Chen, F.H.,
781 2021c. Internal feedbacks forced Middle Holocene cooling on the Qinghai-Tibetan
782 Plateau. *Boreas*.

783 Wang, N., Liu, L., Hou, X., Zhang, Y., Wei, H., Cao, X., 2022. Palynological evidence reveals
784 an arid early Holocene for the northeast Tibetan Plateau. *Climate of the Past* 18, 2381-
785 2399.

786 Weber, Y., De Jonge, C., Rijpstra, W.I.C., Hopmans, E.C., Stadnitskaia, A., Schubert, C.J.,
787 Lehmann, M.F., Sinninghe Damsté, J.S., Niemann, H., 2015. Identification and carbon
788 isotope composition of a novel branched GDGT isomer in lake sediments: Evidence for
789 lacustrine branched GDGT production. *Geochimica et Cosmochimica Acta* 154, 118-129.

790 Weber, Y., Sinninghe Damsté, J.S., Zopfi, J., De Jonge, C., Gilli, A., Schubert, C.J., Lepori, F.,
791 Lehmann, M.F., Niemann, H., 2018. Redox-dependent niche differentiation provides
792 evidence for multiple bacterial sources of glycerol tetraether lipids in lakes. *Proc Natl*
793 *Acad Sci U S A* 115, 10926-10931.

794 Weijers, J.W.H., Schouten, S., van den Donker, J.C., Hopmans, E.C., Sinninghe Damsté, J.S.,
795 2007. Environmental controls on bacterial tetraether membrane lipid distribution in soils.
796 *Geochimica et Cosmochimica Acta* 71, 703-713.

797 Woltering, M., Werne, J.P., Kish, J.L., Hicks, R., Sinninghe Damsté, J.S., Schouten, S., 2012.
798 Vertical and temporal variability in concentration and distribution of thaumarchaeotal
799 tetraether lipids in Lake Superior and the implications for the application of the TEX86
800 temperature proxy. *Geochimica et Cosmochimica Acta* 87, 136-153.

801 Wu, D., Chen, X., Lv, F., Brenner, M., Curtis, J., Zhou, A., Chen, J., Abbott, M., Yu, J., Chen,
802 F., 2018. Decoupled early Holocene summer temperature and monsoon precipitation in
803 southwest China. *Quaternary Science Reviews* 193, 54-67.

804 Wu, J., Yang, H., Pancost, R.D., Naafs, B.D.A., Qian, S., Dang, X., Sun, H., Pei, H., Wang,
805 R., Zhao, S., Xie, S., 2021. Variations in dissolved O₂ in a Chinese lake drive changes in
806 microbial communities and impact sedimentary GDGT distributions. *Chemical Geology*
807 579.

808 Yan, T., Zhao, C., Yan, H., Shi, G., Sun, X., Zhang, C., Feng, X., Leng, C., 2021. Elevational
809 differences in Holocene thermal maximum revealed by quantitative temperature
810 reconstructions at ~30° N on eastern Tibetan Plateau. *Palaeogeography,
811 Palaeoclimatology, Palaeoecology* 570, 110364.

812 Yao, T., Bolch, T., Chen, D., Gao, J., Immerzeel, W., Piao, S., Su, F., Thompson, L., Wada, Y.,
813 Wang, L., Wang, T., Wu, G., Xu, B., Yang, W., Zhang, G., Zhao, P., 2022. The imbalance
814 of the Asian water tower. *Nature Reviews Earth & Environment* 3, 618-632.

815 Zhang, C., Zhao, C., Yu, S.-Y., Yang, X., Cheng, J., Zhang, X., Xue, B., Shen, J., Chen, F.,
816 2022a. Seasonal imprint of Holocene temperature reconstruction on the Tibetan Plateau.
817 *Earth-Science Reviews* 226, 103927.

818 Zhang, E., Chang, J., Cao, Y., Sun, W., Shulmeister, J., Tang, H., Langdon, P.G., Yang, X.,
819 Shen, J., 2017. Holocene high-resolution quantitative summer temperature
820 reconstruction based on subfossil chironomids from the southeast margin of the
821 Qinghai-Tibetan Plateau. *Quaternary Science Reviews* 165, 1-12.

822 Zhang, E., Chang, J., Shulmeister, J., Langdon, P., Sun, W., Cao, Y., Yang, X., Shen, J., 2019a.
823 Summer temperature fluctuations in Southwestern China during the end of the LGM and
824 the last deglaciation. *Earth and Planetary Science Letters* 509, 78-87.

825 Zhang, G., Luo, W., Chen, W., Zheng, G., 2019b. A robust but variable lake expansion on the
826 Tibetan Plateau. *Science Bulletin* 64, 1306-1309.

827 Zhang, W., Wu, H., Cheng, J., Geng, J., Li, Q., Sun, Y., Yu, Y., Lu, H., Guo, Z., 2022b.
828 Holocene seasonal temperature evolution and spatial variability over the Northern
829 Hemisphere landmass. *Nat Commun* 13, 5334.

830 Zhao, B., Castaneda, I.S., Bradley, R.S., Salacup, J.M., de Wet, G.A., Daniels, W.C.,
831 Schneider, T., 2021a. Development of an in situ branched GDGT calibration in Lake 578,
832 southern Greenland. *Organic Geochemistry* 152.

833 Zhao, C., Liu, Z.H., Rohling, E.J., Yu, Z.C., Liu, W.G., He, Y.X., Zhao, Y., Chen, F.H., 2013.
834 Holocene temperature fluctuations in the northern Tibetan Plateau. *Quaternary Research*
835 80, 55-65.

836 Zhao, C., Rohling, E.J., Liu, Z., Yang, X., Zhang, E., Cheng, J., Liu, Z., An, Z., Yang, X.,
837 Feng, X., Sun, X., Zhang, C., Yan, T., Long, H., Yan, H., Yu, Z., Liu, W., Yu, S.-Y., Shen,
838 J., 2021b. Possible obliquity-forced warmth in southern Asia during the last glacial stage.
839 *Science Bulletin* 66, 1136-1145.

840 Zheng, Y., Li, Q., Wang, Z., Naafs, B.D.A., Yu, X., Pancost, R.D., 2015. Peatland GDGT
841 records of Holocene climatic and biogeochemical responses to the Asian Monsoon.
842 *Organic Geochemistry* 87, 86-95.

843 Zhou, W., Yu, S.-Y., Burr, G.S., Kukla, G.J., Jull, A.J.T., Xian, F., Xiao, J., Colman, S.M., Yu,
844 H., Liu, Z., Kong, X., 2010. Postglacial changes in the Asian summer monsoon system:
845 a pollen record from the eastern margin of the Tibetan Plateau. *Boreas* 39, 528-539.

846 Zielinski, G.A., Mershon, G.R., 1997. Paleoenvironmental implications of the insoluble
847 microparticle record in the GISP2 (Greenland) ice core during the rapidly changing

848 climate of the Pleistocene-Holocene transition. Geological Society of America Bulletin
849 109, 547-559.

850

851